ARTICLE

Towards a comprehensive understanding of mesoporosity in zeolite Y at the single particle level

Received 00th January 20xx,
Accepted 00th January 20xx

DOI: 10.1039/x0xx00000x

Zhengxing Qin,[a*] Bo Wang,[a] Natsuko Asano,[b] Lijuan Wang,[a] Yan Zhou,[c] Xinmei Liu,[a] Baojian Shen,[d] Svetlana Mintova,[a,e] Shunsuke Asahina,[b*] Valentin Valtchev[e*]

A full understanding of zeolite mesoporosity is not trivial yet is necessary to understand and optimize the catalytic performance of zeolites. The present work reports an integrated approach for the comprehensive study of zeolite mesoporosity. The comprehensiveness and effectiveness of the methodology is exemplified by the characterization of the hierarchical zeolite Y samples prepared by NH_4F etching. In the present work, usually lacking information of mesopore morphology, connectivity and spacial location, was obtained by the ultra-high-resolution FE-SEM imaging of zeolite cross-section after surface coating with osmium (Os). The ultrahigh-resolution SEM study allowed both: i) the macroscopic documentation of the interconnecting channel-like porosity separating intergrown crystals; and ii) the nano-scale resolving of mesopore spatial distribution within an individual crystal. In addition, the combination of NH_4F etching with state-of-the-art ultra-high-resolution FE-SEM imaging technique proves a powerful methodology to reveal otherwise inaccessible information regarding mesopore formation mechanism. The hiererchical pore structure analysis of zeolite Y is combined with catalytic testing in the dealkylation of 1,3,5 tri-isopropylbenzene for deeper understanding of its physicochemical properties.

.

1. Introduction

Hierarchical zeolites, i.e., zeolites with auxiliary porosity mostly in the mesoporous size range, are intensively studied in recent years, especially in heterogeneous catalysis where the intra-crystalline diffusion is an important issue.[1-3] To identify the most appropriate hierarchical materials for existing and emerging applications, one would expect to have a comprehensive set of data about the porosity properties of zeolite in use, as a detailed insight into the pore architecture are essential because they control transport phenomena and govern selectivity in catalyzed reactions.[4]

The characterization of zeolite porosity is routinely achieved by the application of N_2 or Ar physisorption at cryogenic temperature.[5] Based on the obtained physisorption isotherms, the porosity properties, specific surface area, micropore volume, mesopore volume, pore size distribution, etc., are derived by applying a set of mathematical models (t-plot, BJH, DFT, etc). The presence of mesoporosity is indicated by the isotherms' type and the presence of a specific hysteresis loop.[5] In addition to this routinely available measurement that measures porosity in an indirect way, complementary electron microscopic techniques are also available for the direct visualization of micro-, meso- and macropore networks.[4,6] In this respect, both scanning and transmission electron microscopy are very popularly used for the direct visualization of zeolite porosity.[7,8] In both cases, the presence of pores is clearly reflected by the darker/lighter image contrast difference. In conjunction with image contrast analysis, TEM combined with modelling (electron tomography, ET) permits further the spatial description of meso- and macropores in three-dimensions and the estimation of the amount of open and closed mesopores and pore connectivity.[9]

Despite the well-established complementarity between these macroscopic and microscopic methods, the information collected from these textural characterizations is still limited. Sometimes, apparent contradictory observations have been reported with no coherent agreement on the origin and morphology of the of mesopores. For example, independent studies on related commercial ultra-stable Y (USY) zeolites (CBV series) indicated that the applied steam and acid treatments in one case mainly led to isolated "cavities" and in the other to obvious "channel-like" mesopores.[10-13] Noting that these conflicting conclusions are made based on a set of similarly combined characterization methodologies. Apparently, this can be attributed to some of the obvious difficulties of the current tool kit for the objective characterization of zeolite mesoporosity. For example, conventional TEM and SEM techniques have intrinsic limitations in obtaining the spatial information of mesopores (location, morphology, connectivity) from a 3-dimentional perspective. ET method is powerful, but it is limited to 1~2 thin specimens usually smaller than 100 nm. It provides a limited view of the mesoporosity of the bulk sample. In addition, the studies of zeolite mesoporosity based

[a.] State Key Laboratory of Heavy Oil Processing, College of Chemical Engineering, China University of Petroleum (East China), Qingdao 266580, China
[b.] SEM Application Team, JEOL Ltd., Akisima, Tokyo 196-8558, Japan
[c.] Quantachrome Application Team, Anton Paar China, Shanghai 201103, China
[d.] State Key Laboratory of Heavy Oil Processing; the Key Laboratory of Catalysis of CNPC; College of Chemical Engineering, China University of Petroleum (Beijing), Beijing 102249, China
[e.] Normandie Univ, ENSICAEN, UNICAEN, CNRS, Laboratoire Catalyse et Spectrochimie, 6 Boulevard Maréchal Juin, 14050 Caen, France.

solely on experimental observations present only a one-sided picture of the issue. A more comprehensive understanding of a hierarchical zeolite's porosity properties calls for complementary methods that can provide more objective information about the porosity properties beneath the surface of zeolite crystals and a deep understanding of the mesopore formation mechanisms.

In the present work, the mesopore structure of a 30 wt% NH_4F-treated zeolite Y was studied by combining N_2 physisorption, TEM, and ultrahigh-resolution FE-SEM imaging. By using the NH_4F-treated zeolite as a unique research model, the limitations of conventional SEM and TEM characterizations that non-invasively visualize the surface structure or document the projection of three-dimensional structures was addressed. The unique advantage of ultra-high-resolution FE-SEM imaging to "see" the pores directly from zeolite cross-section was emphasized. In addition, based on the deep understanding of the dissolution behavior of zeolite Y in NH_4F solutions,[4,14,15] the origin of the mysterious "channel-like" mesopores in zeolite Y[10-13] were discussed.

2. Experimental

2.1 Samples preparation

A commercial Y zeolite (Y-54) provided by UOP was used as parent zeolite. Before the fluoride medium etching with NH_4F solution, the starting zeolite was ion-exchanged three times with 1 mol/L aqueous ammonium chloride solution at 353 K using liquid : solid = 20 ratio. The ammonium exchange was carried out for 3 h each time. The obtained zeolite (PY) was treated with a 30 wt % NH_4F (98.0%, Sigma-Aldrich) solution at liquid : solid = 16. The treatment was performed under ultrasonic radiation (USC 600 TH, 45 kHz, VWR) in an ice bath (277 K) for 1 or 5 min. The resulting samples were denoted YF1 and YF2, respectively. The solid products were washed thoroughly and dried.

2.2 Characterization and catalytic testing

X-ray diffraction (XRD) patterns were obtained using a PANalytical X'Pert Pro diffractometer (Cu K_α, 45 kV, 40 mA) with a scanning step of 0.0167° s^{-1}. The Si and Al compositions were analyzed by inductively coupled plasma optical emission (ICP, OPTIMA 4300 DV). Nitrogen physisorption was carried out on a Micromeritics ASAP 2020 automated gas adsorption analyzer. Prior to analysis, the samples were degassed at 373 K for 1 h and 573 K for 10 h. The BET equation was used for determining the specific surface areas. The micropore and mesopore volume were determined using Anton Paar Quantachrome DFT model. The BJH pore size distribution of the parent and the NH_4F treated zeolite Y were obtained from the adsorption and desorption branches of the isotherm.

Scanning electron microscopy (SEM) images of non-coated zeolite surface were taken with JSM-7800F Prime (JEOL) scanning electron microscope equipped with a field emission gun. The acceleration voltage was 0.5 or 1 kV. The cross-section of zeolite samples was prepared by using an IB-19510CP (JEOL) ion Beam cross-section polisher. Transmission electron microscopy (TEM) images were recorded using a JEM-2100 (JEOL) with an accelerated voltage of 200 kV.

Infrared spectra (IR) were recorded using a Nicolet Magna 550-FT-IR spectrometer at 2 cm^{-1} optical resolution. The zeolite powder was pressed into a self-supporting disc (1.6 cm in diameter, ~18 mg) and pretreated in-situ in an IR cell attached to a vacuum line at 723 K (2 K / min) for 4 h down to 10^{-6} Torr. The adsorption of pyridine was performed at 373 K in 1 Torr pyridine gas to reach equilibrium. Then the cell was evacuated at 373-673 K. The amount of pyridine that remained adsorbed after the evacuation was determined using the integrated area of the bands observed at 1545 cm^{-1} and 1454 cm^{-1}, respectively. All spectra were normalized to 20 mg wafers. The extinction coefficients used for pyridine were $\varepsilon(B)_{1545}$=1.3, $\varepsilon(L)_{1450}$=1.5. The zeolite samples were tested in the 1,3,5 tri-isopropylbenzene dealkylation. The catalytic tests were carried out following the conditions reported before.[15]

3. Results

3.1 The parent zeolite Y

The SEM images of the parent zeolite Y used in the present study is shown in Figure 1. The typical morphology of FAU zeolite is clearly distinguishable. The crystal habit is octahedral with multiple twinning polyhedral (Figure 1a-c). The crystal surface is smooth, with the surface growth layer distinguishable (Figure 1d). There are no identifiable mesopores on the crystal surface. This is a phase-pure sample with a high crystallinity (Figure 2). The N_2 physisorption result also shows that this zeolite is a pure microporous sample (Figure 3a).

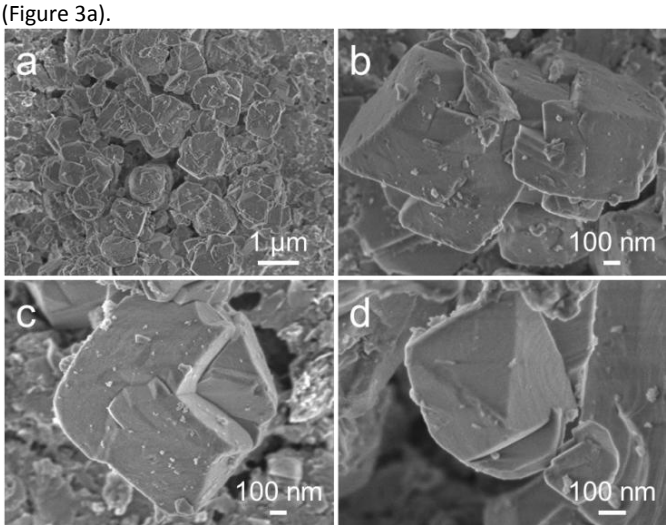

Figure 1 Low (a) and high (b) resolution SEM images of the parent zeolite.

3.2 The NH_4F treated zeolites

The NH_4F treated zeolites remain phase pure and crystalline, with a noticeable decrease in XRD peak intensity compared with the parent sample (Figure 2). The Si/Al ratio of the samples remains unchanged after the NH_4F treatment (Table 1). The results are in agreement with our previous studies.[15-17] On the other hand, the concentration of the NH_4F aq. solution used for fluoride etching was 30 wt% in the present work, which is 5 wt% higher than the one we used previously for opening the sodalite cages of zeolite Y.[15] This

increase in NH_4F concentration changed the dissolution behavior of zeolite Y substantially. The ensuing changes in zeolite mesoporosity were studied in detail.

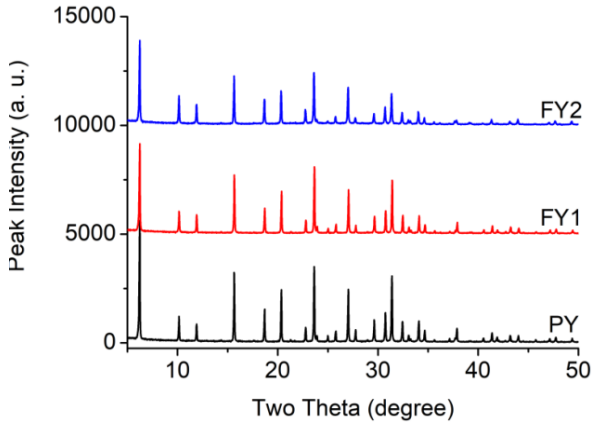

Figure 2 The XRD patterns of the parent zeolite Y (PY) and the samples prepared by NH_4F etching for 1 (FY1) or 5 min (FY2).

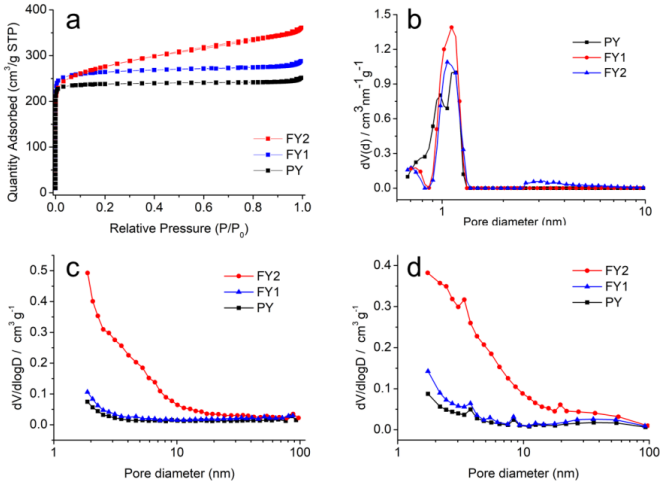

Figure 3 (a) The N_2 physisorption isotherms of the parent and the NH_4F treated zeolite Y samples; (b) The pore size distribution derived from the DFT model; (c, d) The BJH pore size distribution of the parent and the NH_4F treated zeolite Y obtained from the adsorption (c) and desorption (d) branch of the isotherms.

3.2.1. N_2 physisorption characterization of the NH_4F etched samples

N_2 physisorption analysis provides a quantitative evaluation of the bulk porosity of zeolite samples. In addition, the mesopores' features and interconnectivity can be inferred based on the shape of the isotherms.[5] PY exhibits a typical type I isotherm. The adsorption and desorption branches of the isotherm overlap each other throughout the whole P/P_0 range, indicating no mesopores existing. This is also confirmed by data analysis (Table 1). FY1 shows isotherms similar in shape to that of the parent sample (Figure 3a), indicating that this sample remains its microporous characteristic. The mesopore volume of PY and FY1 are essentially the same (Table 1). The rise of the isotherms at a low relative pressure (P/P_0) indicates a noticeably enhanced microporosity. We have shown previously that the increase in micropore volume is the result of the opening of sodalite cages in the case of FAU-Y zeolite.[15]

Table 1 The bulk Si/Al ratio and the porosity data of the parent and NH_4F treated zeolite Y. samples.

Samples	Si/Al_{ICP}[a]	S_{BET}[b]	V_{mic}[c]	S_{meso}[c]	V_{meso}[c]
		m^2g^{-1}	cm^3g^{-1}	m^2g^{-1}	cm^3g^{-1}
PY	2.6	986	0.36	0	0
FY1	2.6	1069	0.39	4	0.02
FY2	2.6	1036	0.33	158	0.19

[a]ICP. [b]BET surface area. [c]Calculated from DFT.

The extension of the NH_4F etching time from 1 min to 5 min leads to a substantial change in the isotherm slop. As can be seen in Figure 3a, the isotherms of FY2 rise linearly with increasing P/P_0 in the range between ca. 0.05 to 1, indicating the presence of plate-like mesopores. The sample has a large mesoporous surface area of 150 m^2g^{-1} (Table 1). It should be noted that the classical relative pressure (P/P_0) range of 0.05-0.3 might not be applicable for the calculation of the B.E.T. surface area of microporous materials. For such samples, the linear range could move to lower P/P_0. In the present case, a P/P_0 range of 0.0003-0.01 is chosen for B.E.T. calculation, according to Rouquerol rules.[18] The mesopore volume of this sample, derived from the difference between the DFT pore volume of 2 nm micropore and 50 nm mesopore, increased by more than 10 times compared to FY1. As far as the mesopore size is concerned, both BJH pore size distributions derived from the adsorption (Figure 3c) and desorption (Figure 3d) branches show a narrow pore size distribution with a similar pore size range between 2-10 nm. There is no hysteresis loop in the isotherms, indicating that all the mesopores are freely accessible to the external surface of zeolite crystals. Later it will be shown that the nitrogen physisorption results truly reflected the structural features of mesopores (pore size, morphology, and connectivity) in NH_4F treated zeolite Y samples, although the spatial location information about the mesoporosity is not available.

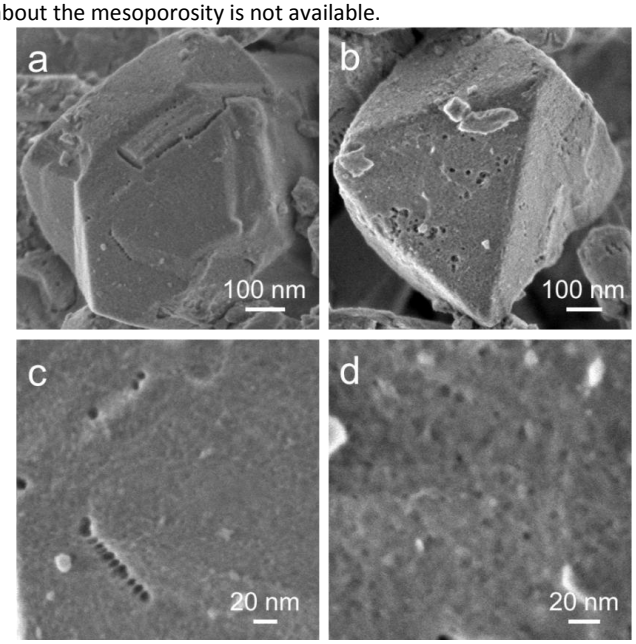

Figure 4 Low (a,b) and high (c,d) magnification SEM images of the FY1 sample.

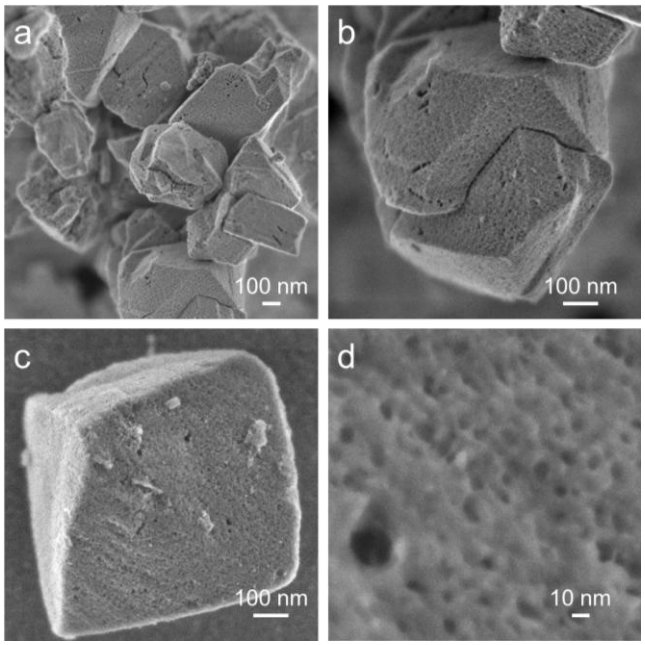

Figure 5 Low (a,b) and high (c,d) magnification SEM images of the FY2 sample.

3.3.2. SEM observation of the external surface of NH_4F etched samples

The SEM was applied to have the information of the crystal morphology and porosity properties of the sample after NH_4F treatment. This technique relies on the signals from the surface of the samples. As shown in Figure 4, the applied NH_4F etching changes obviously the surface morphology of FY1, even though the scheduled etching time was as short as 1 min. The crystal surface is not as smooth as the parent sample (Figure 1). Instead, a few distinct cracks and pits occur on the surface of the treated zeolite crystals. While some of these pores are very small, barely distinguishable under the applied SEM conditions (Figure 4d), a few mesopores are large isolated, with ~10 nm pore opening (Figure 4a-c). Despite the presence of these mesopores on the surface of the crystals (Figure 4), FY1 is classified as a pure microporous zeolite according to its isotherm (Table 1).

The roughening of crystal surface is even more obvious in the case of FY2 (Figure 5), the sample treated in 30 wt% NH_4F solution for 5 min. In this case, distinct cracks separating intergrown crystals apart are clearly observable (Figure 5a, b). Mesopores of various dimensions are densely distributed on each crystal face (Figure 5c, d). This information indicates a substantial etching, in comparison to FY1, as a result of the extended etching in NH_4F solution of high concentration. In our previous work,[15] the parent zeolite was also treated using a 25 wt% NH_4F solution for 5 min. However, there are substantial morphological differences between this sample (Figure 6) and FY2 (Figure 5). In the former case, the treated one retained the morphology of the parent sample (Figure 1). No obvious cracking of intergrown crystals and pores are observed on zeolite surface (Figure 6). These data show clearly that the dissolution behavior of zeolite crystals changes substantially with NH_4F concentration. The increase in NH_4F concentration results in both increase in HF and F^-, which leads to a higher amount of bifluoride species in the end. These species are very active for the dissolution of zeolite framework.[14,19]

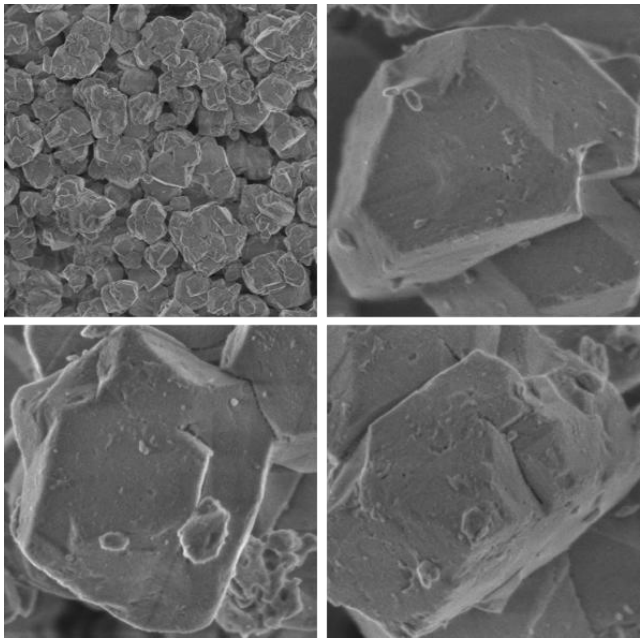

Figure 6 The SEM images of the zeolite Y sample after fluoride etching for 5 min in 25 wt% aqueous NH_4F solution.

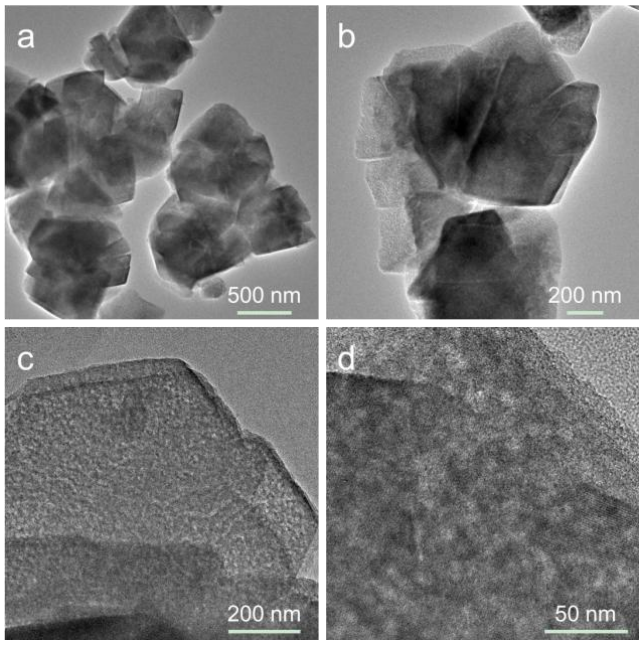

Figure 7 Low (top) and high (bottom) magnification TEM images of the FY2 sample.

3.3.3. TEM observation of the NH_4F etched sample

Since FY1 is considered as a pure microporous sample, FY2 was the only sample selected for TEM inspection. In TEM, the size, density and morphology of mesopores are indicated by the darker-brighter contrast caused by the framework density difference. It can be seen that the FY2 sample looks highly mesoporous, as irregular lighter

areas about 5 nm in size (Figure 7c, d) are distributed uniformly throughout the crystals (Figure 7). In addition to these seemingly uniform mesopores, there is evidence for the deagglomeration of intergrown zeolite crystals (Figure 7a, b). It seems reasonable to consider these pores are similar to one observed on zeolite crystal surface by SEM (Figure 5).

3.3.4. The acidity properties and 1,3,5 tri-isopropylbenzene (TIPB) dealkylation performance of the NH_4F etched samples

As the NH_4F treated zeolites are well-crystallized and highly porous, one may consider an outstanding catalytic performance from these samples. Before doing the catalytic tests, the parent and NH_4F treated zeolite Y samples' acidity was measured by IR monithoring using pyridine as the probe molecule. The Brønsted acidity dominates in the case of the parent sample (Figures 8 a and b). The NH_4F etching leads to a small decrease of Brønsted acidity and an increase in Lewis acidity in FY1. In the case of FY2, the Brønsted acidity decreases substantially, while the Lewis acidity shows a sharp increase (Figures 8 a and b). On the other hand, although the extension of NH_4F etching results in a continuous decrease in the B/L ratio, the summation of Brønsted and Lewis acidity remains almost unchanged (Figure 8c).

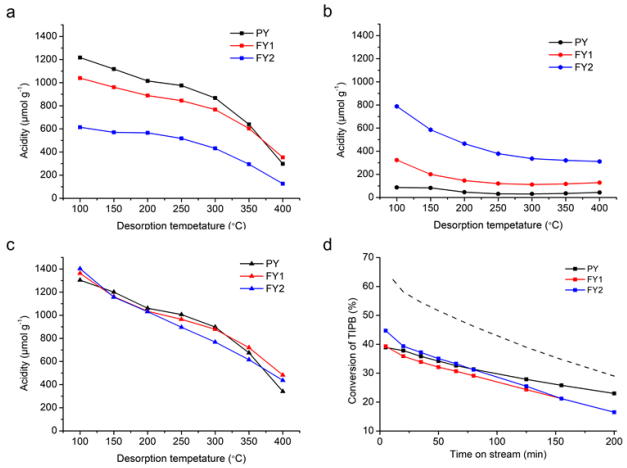

Figure 8 The Brønsted adicity (a), Lewis acidity (b), and summation of Brønsted and Lewis adicity (c) of the parent and NH_4F etched zeolite Y samples. (d) Dealkylation of 1,3,5 tri-isopropylbenzene (TIPB) on the parent and NH_4F etched zeolite Y samples (Reaction temperature = 453 K, W/F° = 0.022 kg h mol^{-1}, P = 0.1 MPa). Note: the dashed line shows the TIPB conversion on another mesoporous Y zeolite prepared by NH_4F etching of the same parent sample.[15] It is used as a reference sample here.

Now that the FY2 zeolite is highly porous and acidic, it was expected that it would show outstanding performance, especially for the catalytic transformation of bulky molecules. Herein, the dealkylation of 1,3,5 tri-isopropylbenzene (TIPB) with a kinetic diameter of 0.95 nm was identified as a model reaction for verification. The size of TIPB is larger than the 0.74 nm large pore opening of zeolite Y. Therefore, it is an appropriate reactant to probe specifically the external and mesoporous surfaces of zeolites.[15] Surprisingly, however, the FY1 sample shows a lower performance during the dealkylation reaction (Figure 8d). FY2, the highly porous one, also shows only a marginally increased dealkylation activity at the beginning of time-on-stream. Moreover, both NH_4F treated samples show a faster deactivation tendency compared to the parent sample. We have shown previously that the TIPB conversion rate increased significantly (Figure 8d) when small intraparticle mesoporosity is added to the same parent zeolite Y sample.[15] However, the data in the present work show clearly that a high mesopore volume, a large mesoporous surface area, and a high amount of acidity are not always a guarantee of high catalytic activity. On the other hand, both FY1 and FY2 show lower 1,3-diisopropylbenzene yield (Figure 9a) and produce higher amount of secondary isomerized products (Figures 9b and c) than PY during the early stage of the catalytic test. Cumene and Benzene yield are also higher in the case of the two FY samples (Figures 9d and e). This is in line with our previous observations,[4] and indicating a subtle change of the microporosity properties on the external and mesoporous surface of zeolite crystals as a result of the opening of zeolite cages.

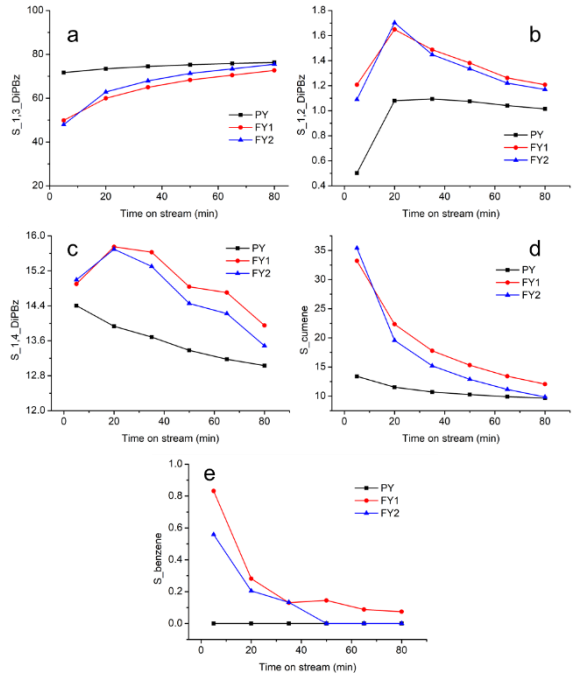

Figure 9 The products selectivity of (a) 1,3-Diisopropylbenzene, (b) 1,2-Diisopropylbenzene, (c) 1,4-Diisopropylbenzene, (d) Cumene, and (e) Benzene as a function of time on stream during the dealkylation of 1,3,5-triisopropylbenzene.

3.3.5. Cross-section ultra-high-resolution FE-SEM analysis of FY2

A deeper insight into the mesoporosity would be helpful to understand better the unexpected catalytic performance of the NH_4F treated zeolites reported above. To fully document the structural features giving rise to the textural properties, it is necessary to study beneath the surface. Here, ultra-high-resolution FE-SEM imaging technology was applied to observe the cross-section of the FY2 sample, with the purpose of having more information about the internal architecture of the secondary porosity beneath the outer surface of zeolite crystals. In order to have a better resolution of the cross-section at high resolution, the sample was first coated with a ~10 nm thick Osmium (Os). Then the cross-section of the Os-coated sample was prepared by Ar ion sputtering following the procedures depicted in Figure 10. The

obtained sample was studied in detail using a JSM-7610FPlus (JEOL) ultrahigh-resolution FE-SEM.

This characterization results in two important observations. First, it reveals an overall highly fragmented pattern suggesting the separation of intergrown crystals along the extended boundaries (Figure 11a, b). This observation is in good agreement with the SEM (Figure 5) and TEM results (Figure 7a, b), while the former provides many more details. Namely, the SEM and TEM show only some plausible evidence for the splitting of intergrown crystals, the direct observation of the cross-section shows unambiguously the presence of multiple cracks penetrated deeply into zeolite crystals. Most of these cracks, with an estimated width of ca. 50 nm, are interconnected with each other. As a result of such cross-linked pores in all directions, the aggregated crystals are formally divided into nanosized domains (Figure 11a, b). The second important finding is about the spatial location of the seemingly homogeneously distributed small mesopores (Figure 7). Namely, a further careful inspection of the cross-section at ultra-high magnification using a LABE (low angle backscattered electrons) model confirmed the presence of small mesopores, but these mesopores are distributed only at the rim of zeolite crystals (Figure 11c, d). The thickness of this surface mesoporous layer is homogeneous, ca. 20 nm thick. The inner part of zeolite crystals is essentially microporous in nature. LABE may escape from near surface of sample. In addition, the voltage of primaly electron energy used as landing voltage was at 3kV. In this case, the information of images are collected from the near surface. Thus, this method is useful to take fine details of sample without the interference of inner information.

Discussion

The indispensability of cross-section imaging

Although both SEM and TEM observations of uncut samples are very useful characterizations for validating the presence of mesoporosity (Figures 4, 5 and 7), both techniques are not adapted to provide information about the 3D morphology and spatial distribution of mesopores. On the other side, physisorption is useful for estimating mesopore size, shape, and connectivity. However, it lacks detailed features about the spatial distribution of mesopores either. Although sophisticated electron tomography (ET) is fantastic for the 3D visualization of mesoporosity,[9] it is a time consuming and labor- intensive process. Besides, the choice of the specimen for ET could be very subjective, as the total amount of zeolite sample used for data collection can be as small as tens of nanometers.[4] Moreover, the application of ET in the present study could be even more challenging, as the NH_4F treated sample, FY2, is not a hierarchical zeolite in the conventional sense.

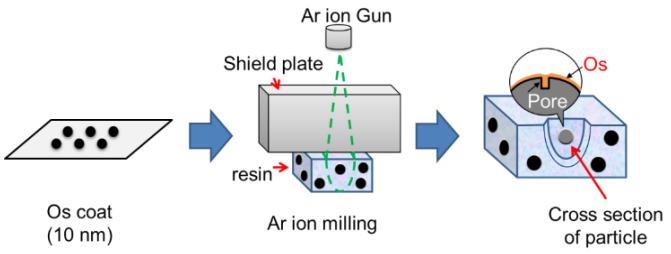

Figure 10 The preparation of the cross-section of zeolite crystals pre-embedded with Os by Ar ion sputtering.

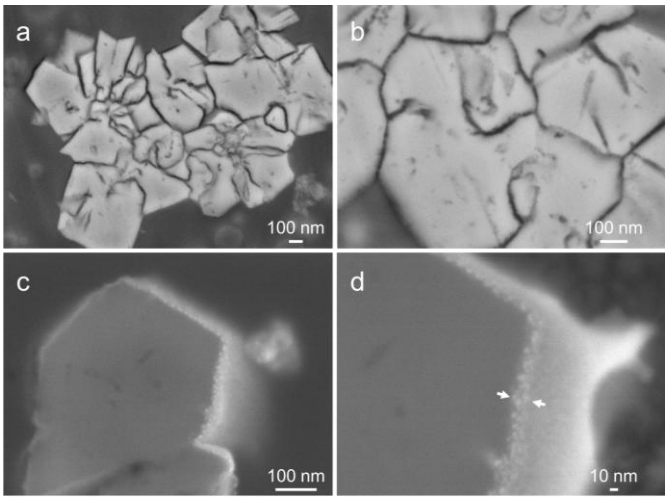

Figure 11 The ultra-high-resolution FE-SEM images of the cross-section of the Os-coated FY2 sample. In Figure 11c and d, Os was penetrated in mesopores. The presence of Os particles in the mesopores was indicated with white arrows.

While the conventional SEM and TEM characterization reflect only the porous characteristics of the NH_4F treated samples without clearly indicating the penetration depth or the spatial distribution of mesopores in zeolite bulk, our study shows a unique advantage of the cross-section imaging technique. By polishing zeolite material with an argon ion beam and then by direct imaging of the secondary porosity network within the cross-section, it is possible to reveal the internal structure with minimal structural damage using ultra-high-resolution scanning electron microscopy (Figure 10 and 11). This allows both the macroscopic capturing of the interstitial porosity among agglomerating crystals (Figure 11a, b) and the microscopic resolving of local structural details within an individual crystal at the nano-scale (Figure 11c, d). This observation demonstrates the lack of mesopores in the bulk of crystals. Also, it reveals the ubiquitous interconnectivity between the interstitial mesoporous networks. This valuable information helps explain the knowledge gap between the SEM, TEM, and N_2 physisorption results. As an easy-to-use technique, we expect a prosperous future for the direct imaging of the cross-section of many other (nano)structured hierarchical zeolites, such as house-of-card zeolites, intraparticle mesoporous zeolites, etc.

The deep insight into the inner architecture of the secondary porosity is very helpful for understanding the unexpected low catalytic performance of the NH_4F treated samples during the TIPB dealkylation. As revealed by the cross-section imaging, the engineering of zeolite crystals by NH_4F etching only results in a substantial dissolution of the surface layer of zeolite crystals. This intensive and localized surface etching deteriorates the surface framework structures and decreases the Brønsted zeolite acidity (Figures 8a and b). However, it fails to introduce a substantial amount of intra-particle mesoporosity in the bulk of zeolite crystals.

As a result, although the external surface area and the mesopore volume increase substantially (Table 1), there is no pathway for the efficient transport of bulky molecules into the inner volume of zeolite crystals. Logically, this only results in a small increase in the TIPB conversion rate. Meanwhile, the broken framework tetrahedral connections produce many surface defect sites (silanol groups). These silanols are very favorable for coke formation.[20] As a result, both NH_4F treated samples show a higher deactivation rate compared to the parent sample (Figure 8 d).

An alternative interpretation of the channel-like secondary pores

We have noticed the presence of many channel-like pores in the volume of the NH_4F treated zeolite Y (Figure 11a, b). The track of these channels is irregular. Most of them are interconnected, separating the bulky zeolite into several smaller domains. The presence of such interconnected "superhighways" would be appropriate from the diffusion perspective.[2,21] On the other hand, the origin of such channels remains to be elucidated. The dissolution of zeolite seems to proceed in such a way that the etchant removes the local framework atoms along the width direction and, at the same time, extends the dissolution front along the length direction. The diameter of the channels, ~ 50 nm in width, is approximately the size of 20 zeolite unit cells. When taking the length scale of the channels into consideration, one can count that several hundreds of unit cells are completely removed following particular directional guidance to build such a broad channel system. Similar channel-like mesopores are also ubiquitously observed in dealuminated zeolite Y crystals.[13] Yet, no satisfactory justification for such "channel-like" mesopores has been approved.

Structurally, it would be difficult to imagine how this happened if we assume that the zeolite crystals, as shown in Figure 11, are complete pieces and indivisible in architecture. Therefore, we provide a tentative interpretation for the origin of the "channel-like" mesopores that can be the grain boundary. Namely, the "channels" are originated from the extensive demetallation along the interface of the intergrown twins. This is based on the unique characteristic of NH_4F etching, which is able to remove unbiasedly Si and Al from the zeolite framework and starts preferentially from framework imperfections.[17,20] In addition, the presence of twin boundaries is common (Figure 12) in Y zeolite crystals.[22-24] The strain of the twisted framework coordination at the interface is believed to be favorable for the hydrolysis of the Si-O-Al bonds. We have previously noticed this phenomenon during the chemical etching of MOR and MFI.[17,25] In the present work, we further addressed this in the case of FAU.

Inspired by the findings, we have treated a home-made zeolite Y sample with an alkaline solution for verification.[26] The parent zeolite Y sample in its Na-form was treated by 10 wt% KOH solution at 363 K for 1h under stirring, using solid-to-liquid ratio of 1:10. The base leaching did not create any intraparticle mesopores in roundish shape. As expected, however, irregularly stretched lines indicating the presence of interface cracks can be seen clearly in the alkaline treated Y zeolite (Figure 13). The fact that zeolite subunits can be separated along grain boundary by dealumination, desilication, and demetallation shows unambiguously that such extended crystal imperfections can ubiquitously serve as superior access for the post-synthesis engineering of zeolite (decrease crystal domain size, adding a new channel system inside bulk zeolite crystals, modifying crystal strains and defects concentrations, etc). As far as the grain boundary is concerned, the interface may not limit to the classical twinning of the same type of zeolite, but could be extended to the intergrowth of different topological structures.[27-30]

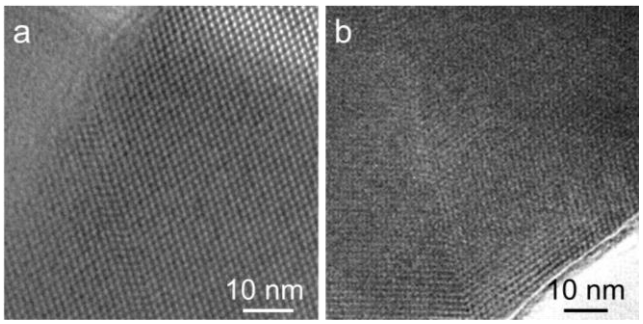

Figure 12 High-resolution TEM images showing the stacking fault (a) and typical twin interface (b) in zeolite Y.

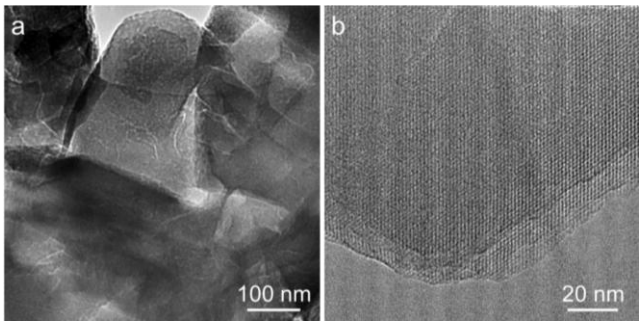

Figure 13 Low (a) and high-resolution (b) TEM images showing the intra-particle cracks induced by alkaline treatment.

Conclusions

The present work shows how the usage of complementary characterization techniques enabled closing the understanding gap concerning the location and structure of mesopores in zeolites. By using the NH_4F treated zeolite Y samples as a rare research model, the secondary porosity of these zeolites was comprehensively studied by a synergistic combination of nitrogen physisorption and electron microscopy techniques. The classic combination of physisorption analysis and conventional SEM/TEM visualization was insufficient for determining the mesoporosity's morphology, connectivity, and spatial location. The knowledge gap was filled by the ultra-high-resolution FE-SEM imaging of zeolite cross-section after surface coating with Os. The latter technique provides detailed spatial information of the mesopore network, which is not reachable by other methods. The instrumental observation was rationalized based on the deep understanding of zeolite dissolution behavior in NH_4F solutions. The deep insight into the mesoporosity properties helps to rationalize the

unexpected low catalytic activity of the NH_4F treated zeolites in the dealkylation of 1,3,5 tri-isopropylbenzene.

Conflicts of interest

There are no conflicts to declare.

Acknowledgements

Z.Q. acknowledges the support from NSFC 22178389, 21706285; S.M. acknowledges the support from NSFC 21975285 and Thousand Talents Program for Foreign Experts (WQ20152100316); Z.Q. and S.M. acknowledge the support from NSFC 21991090, NSFC21991091. V.V. acknowledges the financial support of Carnot Institute (Energie et Systeme de Propulsion) for the 3DNanoZET project and the LABEX EMC program with the reference ANR-11-EQPX-0020. The authors acknowledge funding from the Sino-French joint laboratory "Zeolites".

Notes and references

1 J. Perez-Ramirez, C. H. Christensen, K. Egeblad, C. H. Christensen, J. C. Groen, Hierarchical zeolites: enhanced utilisation of microporous crystals in catalysis by advances in materials design. *Chem. Soc. Rev.* **2008**, *37*, 2530-2542.

2 P. Peng, Z. F. Yan; S. Mintova, X. H. Gao, Diffusion and catalyst efficiency in hierarchical zeolite catalysts. *Natl.Sci.Rev.* **2020**. Doi: 10.1093/nsr/nwaa184

3 L. H. Chen, M. H. Sun, Z. Wang, W. Yang, Z. Xie, B. L. Su, Hierarchically Structured Zeolites: From Design to Application. *Chem. Rev.* **2020**, *120*, 11194-11294.

4 Z. Qin, S. Zeng, G. Melinte, T. Bučko, M. Badawi, Y. Shen, J.-P. Gilson, O. Ersen, Y. Wei, Z. Liu, X. Liu, Z. Yan, S. Xu, V. Valtchev and S. Mintova, Understanding the Fundamentals of Microporosity Upgrading in Zeolites: Increasing Diffusion and Catalytic Performances, *Advanced Science*, 2021, **8**, 2100001.

5 M. Thommes, K. Kaneko, A. V. Neimark, J. P. Olivier, F. Rodriguez-Reinoso, J. Rouquerol, K. S. Sing, Physisorption of gases, with special reference to the evaluation of surface area and pore size distribution (IUPAC Technical Report). *Pure Appl. Chem.*, **2015**, *87*, 1051-1069.

6. Y. Shen, Z. Qin, S. Asahina, N. Asano, G. Zhang, S. Qian, Y. Ma, Z. Yan, X. Liu and S. Mintova, The inner heterogeneity of ZSM-5 zeolite crystals, *Journal of Materials Chemistry A*, 2021, **9**, 4203-4212.

7 A. Janssen, A. Koster, K. P. De Jong, On the shape of the mesopores in zeolite Y: a three-dimensional transmission electron microscopy study combined with texture analysis. *J. Phys. Chem. B* **2002**, *106*, 11905-11909.

8 X. Zhang, D. Liu, D. Xu, S. Asahina, K. A. Cychosz, K. V. Agrawal, Y. Al Wahedi, A. Bhan, S. Al Hashimi, O. Terasaki, Synthesis of self-pillared zeolite nanosheets by repetitive branching. *Science* **2012**, *336*, 1684-1687.

9 Y. Wei, T. E. Parmentier, K. P. De Jong, J. Zečević, Tailoring and visualizing the pore architecture of hierarchical zeolites. *Chem. Soc. Rev.* **2015**, *44*, 7234-7261.

10 A. H. Janssen, A. J. Koster, K. P. De Jong, Three-dimensional transmission electron microscopic observations of mesopores in dealuminated zeolite Y. *Angew. Chem. Int. Ed.* **2001**, *40*, 1102-1104.

11 K. P. De Jong, J. Zečević, H. Friedrich, P. E. De Jongh, M. Bulut, S. Van Donk, R. Kenmogne, A. Finiels, V. Hulea, F. Fajula, Zeolite Y crystals with trimodal porosity as ideal hydrocracking catalysts. *Angew. Chem. Int. Ed.* **2010**, *49*, 10074-10078.

12 J. Zečević, C. J. Gommes, H. Friedrich, P. E. De Jongh,; K.P. De Jong, Mesoporosity of zeolite Y: quantitative three-dimensional study by image analysis of electron tomograms. *Angew. Chem. Int. Ed.* **2012**, *51*, 4213-4217.

13 J. Kenvin, S. Mitchell, M. Sterling, R. Warringham, T. C. Keller, P. Crivelli, J. Jagiello, J. Pérez-Ramírez, Quantifying the complex pore architecture of hierarchical faujasite zeolites and the impact on diffusion. *Adv. Funct. Mater.* **2016**, *26*, 5621-5630.

14 Y. Shen, M. Xu, j. Li, Z. Qin, C. Wang, S. Mintova and X. Liu, Preparation of core–shell-like zeolites by diffusion controlled chemical etching, *Inorganic Chemistry Frontiers*, 2021, **8**, 2144-2152.

15 Z. Qin, K. A. Cychosz, G. Melinte, H. El Siblani, J. P. Gilson, M. Thommes, C. Fernandez, S. Mintova, O. Ersen, V. Valtchev, Opening the Cages of Faujasite-Type Zeolite. *J. Am. Chem. Soc.* **2017**, *139*, 17273-17276.

16 Z. Qin, J.-P. Gilson and V. Valtchev, Mesoporous zeolites by fluoride etching, *Current Opinion in Chemical Engineering*, 2015, **8**, 1-6.

17 Z. Qin, G. Melinte, J. P. Gilson, M. Jaber, K. Bozhilov, P. Boullay, S. Mintova, O. Ersen, V. Valtchev, The mosaic structure of zeolite crystals. *Angew. Chem. Int. Ed.* **2016**, *128*, 15273-15276.

18 P. Llewellyn, F. Rodriguez-Reinoso, J. Rouquerol, N. Seaton, Characterization of porous solids VII. *Stud. Surf. Sci. Catal.* **2007**, *160*, 49-56.

19 Z. Qin, L. Lakiss, J. P. Gilson, K. Thomas, J. M. Goupil, C. Fernandez and V. Valtchev, Chemical Equilibrium Controlled Etching of MFI-Type Zeolite and Its Influence on Zeolite Structure, Acidity, and Catalytic Activity, *Chemistry of Materials*, 2013, **25**, 2759-2766.

20 Z. Qin, L. Pinard, M. A. Benghalem, T. J. Daou, G. Melinte, O. Ersen, S. Asahina, J.P. Gilson, V. Valtchev, Preparation of Single-Crystal "House-of-Cards"-like ZSM-5 and Their Performance in Ethanol-to-Hydrocarbon Conversion. *Chem. Mater.* **2019**, *31*, 4639-4648.

21 R. Bai, Y. Song, Y. Li, J. Yu, Creating hierarchical pores in zeolite catalysts. *Trends Chem.* **2019**, *1*, 601-611.

22 Y. Sasaki, T. Suzuki, Y. Takamura, A. Saji, H. Saka, Structure analysis of the mesopore in dealuminated zeolite Y by high resolution TEM observation with slow scan CCD camera. *J. Catal.* **1998**, *178*, 94-100.

23 L. Han, T. Ohsuna, Z. Liu, V. Alfredsson, T. Kjellman, S. Asahina, M. Suga, Y. Ma, Oleynikov, P.; Miyasaka, K. Structures of Silica-Based Nanoporous Materials Revealed by Microscopy. *Z. Anorg. Allg. Chem.* **2014**, *640*, 521-536.

24 I. Kumakiri, Y. Sasaki, W. Shimidzu, K. Hashimoto, H. Kita, T. Yamaguchi, S. i. Nakao, Micro-structure change of polycrystalline FAU zeolite membranes during a hydrothermal synthesis in a dilute solution. *Microporous Mesoporous Mat.* **2018**, *272*, 53-60.

25 Z. Qin, L. Hafiz, Y. Shen, S. Van Daele, P. Boullay, V. Ruaux, S. Mintova, J. P. Gilson, V. Valtchev, Defect-engineered zeolite porosity and accessibility. *J. Mater. Chem. A* **2020**, *8*, 3621-3631.

26 Z. Qin, B. Shen, Z. Yu, F. Deng, L. Zhao, S. Zhou, D. Yuan, X. Gao, B. Wang, H. Zhao, A defect-based strategy for the preparation of mesoporous zeolite Y for high-performance catalytic cracking, Journal of Catalysis. *J. Catal.* **2013**, *298*, 102-111.

27 V. Alfredsson, T. Ohsuna, O. Terasaki, J. O. Bovin, Investigation of the Surface Structure of the Zeolites FAU and EMT by High-Resolution Transmission Electron Microscopy. *Angew. Chem. Int. Ed.* **1993**, *32*, 1210-1213.

28 M. Audier, J.M. Thomas, J. Klinowski, D. A. Jefferson, L. A. Bursill, Twinning in zeolite Y. The conversion of faujasite into a new zeolite structure. *J. Phys. Chem.* **1982**, *86*, 581-584.

29 M. W. Anderson, K. S. Pachis, F. Prébin, S. W. Carr, O. Terasaki, T. Ohsuna, V. Alfreddson, Intergrowths of cubic and hexagonal polytypes of faujasitic zeolites. *J. Chem. Soc., Chem. Commun.*

1991, 1660-1664.
30 N. S. John, S. M. Stevens, O. Terasaki, M. W. Anderson, Evolution of surface morphology with introduction of stacking faults in zeolites. *Chem. Eur. J.* **2010**, *16*, 2220-2230.